Supporting Information

Guest control of structure in porous organic cages

Marc A. Little, Samantha Y. Chong, Marc Schmidtmann, Tom Hasell, and Andrew I. Cooper

Chemistry Department and Centre for Materials Discovery, University of Liverpool, Crown Street, Liverpool, L69 7ZD, UK.

Table of Contents

1.1. Materials

1,3,5-Triformylbenzene was purchased from Manchester Organics, UK. All other chemicals were purchased from Sigma-Aldrich and used as received, unless otherwise stated. **CC3**-*R*,[1] and **CC4**-*R*,[2] were prepared according to methods previously described.

1.2. Characterization and Analysis

NMR. Solution ^{1}H NMR spectra were recorded at 400.13 MHz using a Bruker Avance 400 NMR spectrometer.

Thermogravimetric Analysis. TGA analysis was carried out using a Q5000IR analyzer (TA instruments) with an automated vertical overhead thermobalance. The samples were heated at the rate of 10 °C /min.

Single Crystal X-Ray Diffraction. Solvated single crystals, isolated from the crystallisation solvent mixture, were rapidly mounted on a MiTeGen loop and flash cooled to 100 K under a dry nitrogen gas flow. Single crystal X-ray data were measured on a Rigaku MicroMax-007 HF rotating anode diffractometer (Mo-Kα radiation, λ = 0.71073 Å, Kappa 4-circle goniometer, Rigaku Saturn724+ detector). Empirical absorption correction using equivalent reflections was performed with the program SADABS.[3] Structure were solved with SHELXD,[4] or by direct methods using SHELXS,[4] and reined by full-matrix least squares on F^2 by SHELXL-97,[4] interfaced through the programme OLEX2.[5] In general all non-H atoms were refined anisotropically; H atoms were fixed in geometrically estimated positions using the riding model. For full detail of structural refinement, displacement ellipsoid plots, crystal packing diagrams and for further details of variable temperature studies performed on individual crystals see **section 1.3** and **1.7**.

Gas Sorption Analysis. Surface areas were measured by nitrogen adsorption and desorption at 77.3 K. Powder samples were degassed offline at 100 °C for 15 h under dynamic vacuum (10-5 bar) before analysis, followed by degassing on the analysis port under vacuum, also at 100 °C. Isotherms were measured using Micromeritics 2020, or 2420 volumetric adsorption analyzer.

Laboratory powder X-ray diffraction (PXRD). Patterns were collected on a Bruker D8 Advance diffractometer producing Ge-monochromated Cu $K\alpha_1$ radiation equipped with a LynxEye position sensitive detector. The samples were contained in 1 mm diameter special glass capillaries and spun during data collection to improve powder averaging. Data were collected over the range $4 \leq 2\theta \leq 50°$

with a step size of 0.01° over 11 hrs using a variable counting time strategy. Le Bail fitting of the PXRD data was carried out using *TOPAS-Academic*.[6]

Scanning Electron Microscopy. Imaging of the crystal morphology was achieved using a Hitachi S-4800 cold Field Emission Scanning Electron Microscope (FE-SEM). Samples were prepared by depositing dry crystals on 15 mm Hitachi M4 aluminum stubs using an adhesive high purity carbon tab before coating with a 2 nm layer of gold using an Emitech K550X automated sputter coater. Imaging was conducted at a working distance of 8 mm and a working voltage of 3 kV using a mix of upper and lower secondary electron detectors.

1.3 Single Crystal X-ray Crystallography for CC3β

CC3-*R* (300 mg) was dissolved in CH_2Cl_2 (60 mL), to this Et_2O (300 mL) was added. Nitrogen was flowed over the solvent mixture and after 2 days large needle shaped crystal of **CC3**-*R*·3(Et_2O)·CH_2Cl_2 formed, **Figure S1**. After 7 days all of the solvent had evaporated, the crystals were collected and dried in a vacuum oven at 100 °C for 16 hours (100% yield). Repeating the crystallisation using $CHCl_3$/Et_2O instead of CH_2Cl_2/Et_2O resulted in the formation of phase pure crystals of **CC3**α.

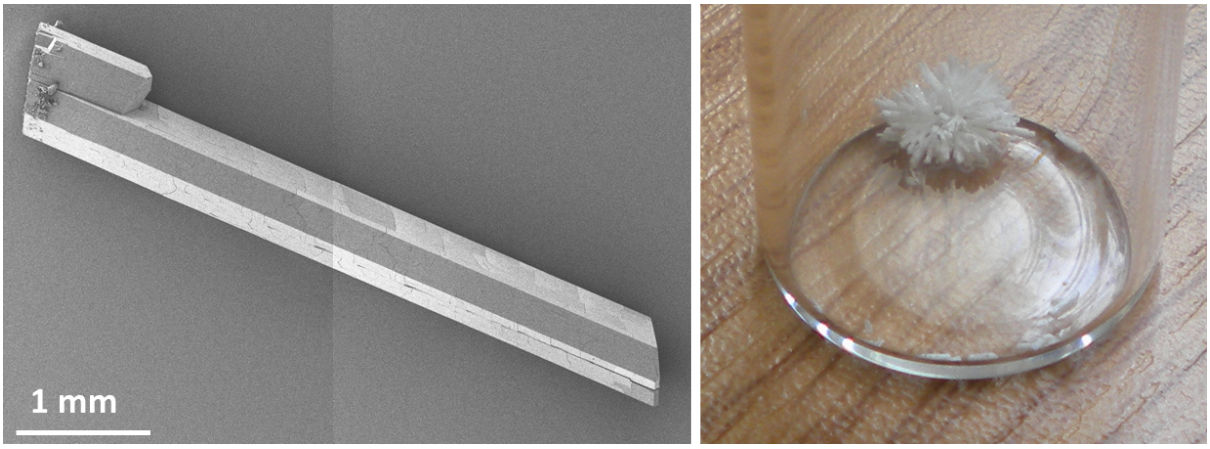

Figure S1. Crystal habit of **CC3**-*R*·3(Et_2O)·CH_2Cl_2.

Single Crystal Experimental Procedure. A single crystal was selected from a sealed sample vial containing residual Et_2O and CH_2Cl_2 and immediately flash frozen under a dry nitrogen gas steam at 100 K. A full data set was recorded, this was refined as **CC3**-*R*·(Et_2O)$_3$·CH_2Cl_2. The same single crystal was heated under the dry nitrogen gas flow to 300 K. Unit cells were determined at 20 K intervals during the heating phase (**Figure S2**). Once the sample had reached 300 K a full data set was recorded, this was subsequently determined to be **CC3**β, and is referred to as **CC3**β-300K hereafter. On completion of the full data set recorded at 300 K the same single crystal was heated to 400 K,

again unit cells were determined at 20 K intervals (**Figure S2**). The full data set that was recorded at 400 K, referred to as **CC3**β-400K, was determined to be structurally almost identical to **CC3**β-300K (**Figure S2**), hence only the 300 K collection is discussed in the main text. The same single crystal was then cooled under a dry nitrogen gas stream to 100 K, and a further full data collection was made. This was subsequently determined to be **CC3**β·(N_2)7.5 with nitrogen being the most likely candidate to account for the disordered residual electron density found for the crystal lattice.

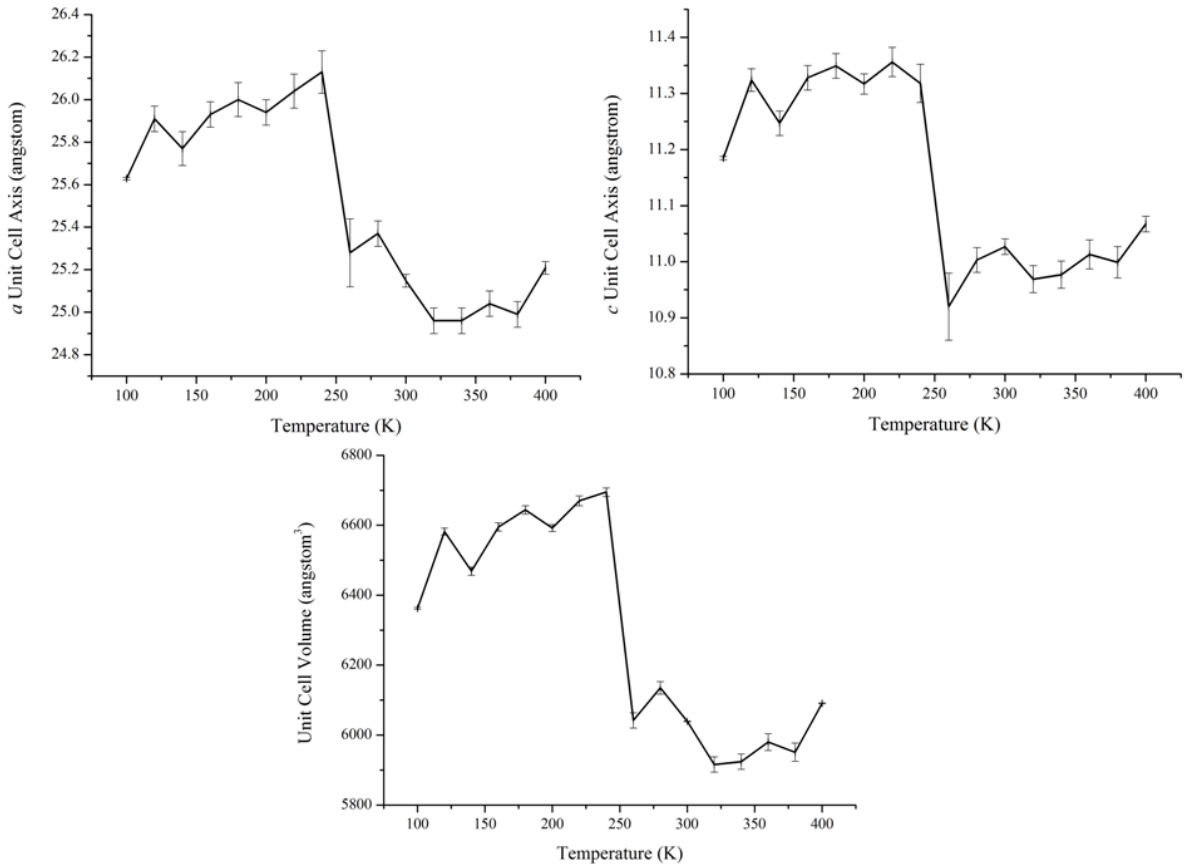

Figure S2. Plot showing the change in the unit cell parameters *a*, *c* and *V* over the course of the *in situ* heating phase of the single study of **CC3**-*R*·3(Et_2O)·CH_2Cl_2 under a dry nitrogen gas stream.

Refinement Notes for CC3-*R*·(Et_2O)3·CH_2Cl_2. The structure was solved and refined in the trigonal space group *R*3. The crystal was weakly diffracting and a 0.85 Å resolution limit was applied during integration. The Et_2O solvate was disordered, DFIX bond restraints were used to restrain C-C and C-O bond lengths and a group DELU restraint was used. The CH_2Cl_2 solvate located in the intrinsic cavity of the cage was severely disordered over a number of positions. This was refined with restraints on 1,2 and 1,3 bond distance using DFIX and DANG restraints respectively, a group DELU restraint was used. The exact location and occupancy of the CH_2Cl_2 should be regarded as tentative. For a displacement ellipsoid plot of the asymmetric unit see **Figure S3**.

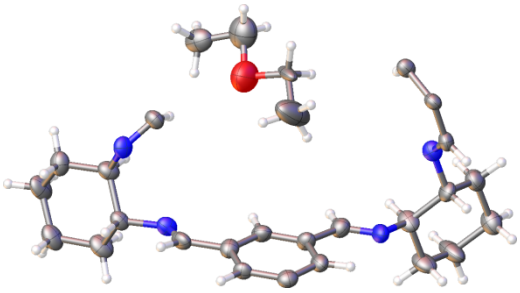

Figure S3. Displacement ellipsoid plot from the single crystal structure **CC3**-*R*·(Et_2O)3·CH_2Cl_2. Disordered CH_2Cl_2 omitted for clarity. Ellipsoids displayed at 50 % probability level.

Refinement Notes for CC3β-300K. The structure was solved and refined in the trigonal space group *P*3. A 1 Å resolution limit was applied during integration. The asymmetric unit for **CC3**β-400K comprises three cage fragments from three crystallographically distinct **CC3**-*R* molecules. No constraint or restraints were used during refinement. For a displacement ellipsoid plot of the asymmetric unit see **Figure S4**.

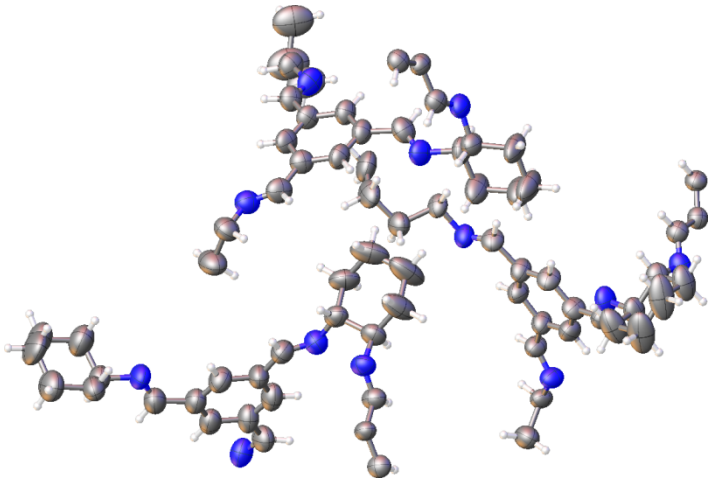

Figure S4. Displacement ellipsoid plot from the single crystal structure **CC3**β-300K. Ellipsoids displayed at 50 % probability level.

Refinement Notes for CC3β-400K. The structure was solved and refined in the trigonal space group *P*3. A 1 Å resolution limit was applied during integration. The asymmetric units for **CC3**β-400K comprises three cage fragments from three crystallographically distinct **CC3**-*R* molecules. No constraint or restraints were used during refinement. For a displacement ellipsoid plot of the asymmetric unit see **Figure S5**.

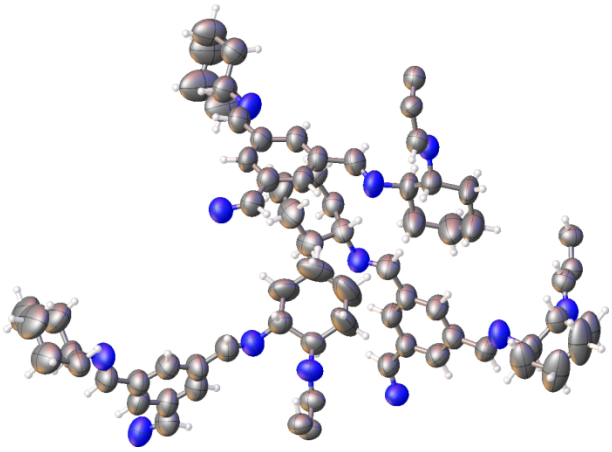

Figure S5. Displacement ellipsoid plot from the single crystal structure **CC3**β-400K. Ellipsoids displayed at 50 % probability level.

Refinement Notes for CC3β·7.5 (N_2). The structure was solved and refined in the trigonal space group *P*3. A 0.9 Å resolution limit was applied during integration. The asymmetric units for **CC3**β·7.5 (N_2) comprises three cage fragments from three crystallographically distinct **CC3**-*R* molecules. Residual electron density found in difference map was assigned as nitrogen, the most likely candidate after cooling the single crystal *in situ* from 400 K to 100 K under a dry nitrogen gas stream. Although the exact location and occupancies for these N_2 molecules should be regarded as tentatively assigned. For a displacement ellipsoid plot of the asymmetric unit see **Figure S6**. The crystal structure of the nitrogen loaded structure shares structural similarities with **CC3β** although one notable difference is an increase in the tetrahedral volume calculated for the three crystallographically independent cages from that of the solvate despite a contraction of the cell volume (**Figure S10**, **Table S2**). Evaluating the solvent accessible surface area for **CC3**β reveals that when using a probe radius of 1.55 Å (kinetic probe radius for nitrogen) the blue cage is inaccessible unlike the red and green cages that remain accessible. This trend is the same for the nitrogen-loaded structure following *in silico* removal of the nitrogen molecules. Comparing these to the solvent accessible surface area calculated for an *in silico* desolvated **CC3**-*R*·3(Et_2O)·CH_2Cl_2 reveals there is a difference between the connectivity in the what would be blue cage in **CC3**β. In order to evaluate if the solvate was able to leave the blue cage of **CC3**β a proton NMR was recorded on crystalline samples desolvated at 300 K and 400 K (**Figure S7**). The results reveal that CH_2Cl_2 and Et_2O were undetectable in the ^{1}H NMR once the crystals had subjected to these conditions. This may indicate that the blue cages only adopts its final, formally inaccessible, conformation observed in **CC3**β once the solvate has been removed, or is able to undergo dynamic motion to uptake and release guests.

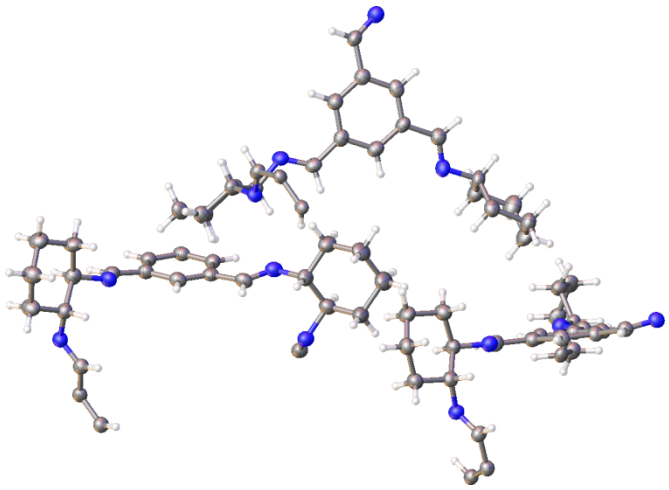

Figure S6. Displacement ellipsoid plot from the single crystal structure CC3β·7.5 (N_2). Ellipsoids displayed at 50 % probability level. Isotropically refined N_2 omitted for clarity.

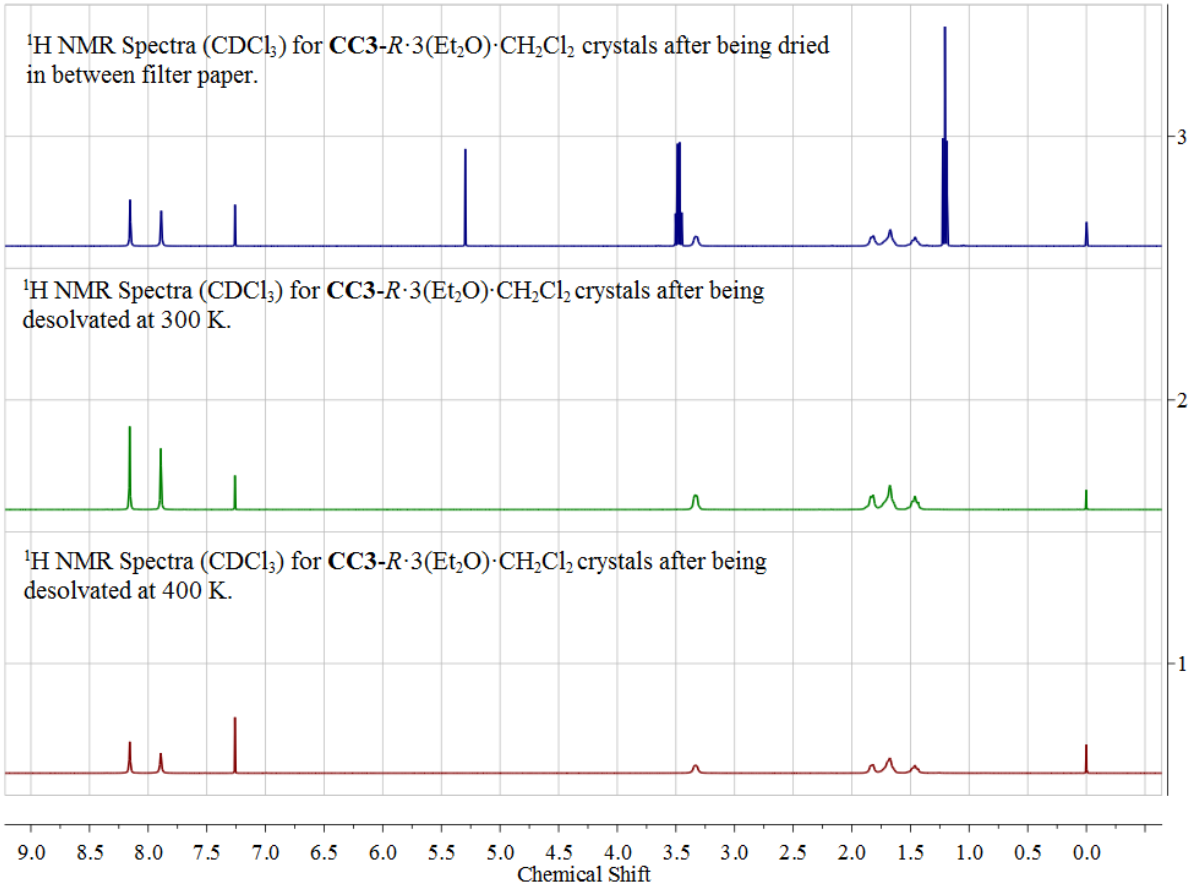

Figure S7. ^{1}H NMR data was recorded on solvated crystal and crystalline material that had been desolvated at 300 K and at 400 K then dissolved in $CDCl_3$.

Table S1. Single crystal X-ray crystallography refinement details for **CC3**-*R*·3(Et_2O)·CH_2Cl_2, and **CC3**β.

Sample Reference	**CC3**-*R*-*R*·3(Et_2O)·CH_2Cl_2	**CC3**β-300K	**CC3**β-400K	**CC3**.7.5(N_2)
Collection *T*	100 K	300 K	400 K	100 K
Formula	$C_{85}H_{116}Cl_2N_{12}O_3$	$C_{72}H_{84}N_{12}$	$C_{72}H_{84}N_{12}$	$C_{72}H_{84}N_{27}$
Mr	1424.75	1117.51	1117.51	1327.66
Crystal Size (mm)	0.43x0.19x0.16	0.43x0.19x0.16	0.43x0.19x0.16	0.43x0.19x0.16
Crystal Colour	colourless	colourless	colourless	colourless
Crystal System	Trigonal	Trigonal	Trigonal	Trigonal
Space Group	*R*3	*P*3	*P*3	*P*3
a = *b* [Å]	25.629(3)	25.148(2)	25.208(2)	25.256(1)
c [Å]	11.185(2)	11.0268(7)	11.0674(7)	11.0068(5)
V [Å^3]	6363(1)	6039.4 (6)	6090.7(6)	6080.1(5)
Z	3	3	3	3
Z'	1	3	3	3
D_{calcd} [g cm^{-3}]	1.118	0.922	0.914	1.088
μ[mm^{-1}]	0.129	0.055	0.055	0.070
F(000)	2313	1800	1800	2115
2θ range [°]	4.04 – 46.50	1.86 - 41.84	4.12 - 41.62	3.72 – 46.58
Reflections collected	14584	36665	37467	41937
Independent reflections, R_{int}	3644, 0.0575	7893, 0.0709	7895, 0.0626	9832, 0.0767
Obs. Data [I > 2σ]	3527	6054	5267	8425
Data / restraints / parameters	3644/31/319	7893/0/757	7893/0/757	9832/7/833
Final R1 values (I > 2σ(I))	0.1095	0.0689	0.0576	0.0642
Final *wR*(F^2) values ($I > 2\sigma(I)$)	0.3007	0.1683	0.1383	0.1723
Final R1 values (all data)	0.1110	0.0959	0.0985	0.0642
Final wR(F2) values (all data)	0.3020	0.1884	0.1637	0.1850
Goodness-of-fit on F^2	1.139	1.065	1.019	1.029
Largest diff. peak and hole [e.A-3]	0.545/-0.627	0.237/-0.204	0.156/-0.164	0.473/-0.303
CCDC	991214	991216	991217	991215

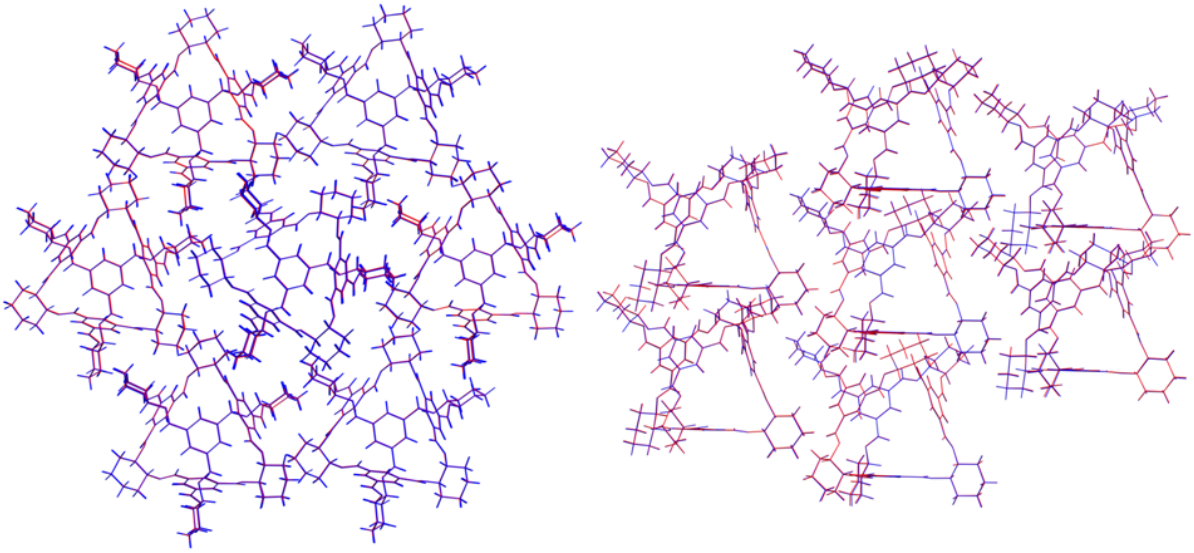

Figure S8. Structure comparison for single crystal structures for **CC3**β recorded at 300 K (red) and 400 K (blue).

Tetrahedral Volume Calculation. Each **CC3**-*R* can be viewed as a tetrahedron when considering the connectivity between the four phenyl rings. This enables an approximate volume for each **CC3**-*R* to be calculated from the single crystal structures of **CC3**-*R*·3(Et_2O)·CH_2Cl_2 (i), **CC3**β-300K (ii), **CC3**β-400K (iii) and **CC3**β.7.5(N_2) (iv) using the Cayley-Menger determinant.

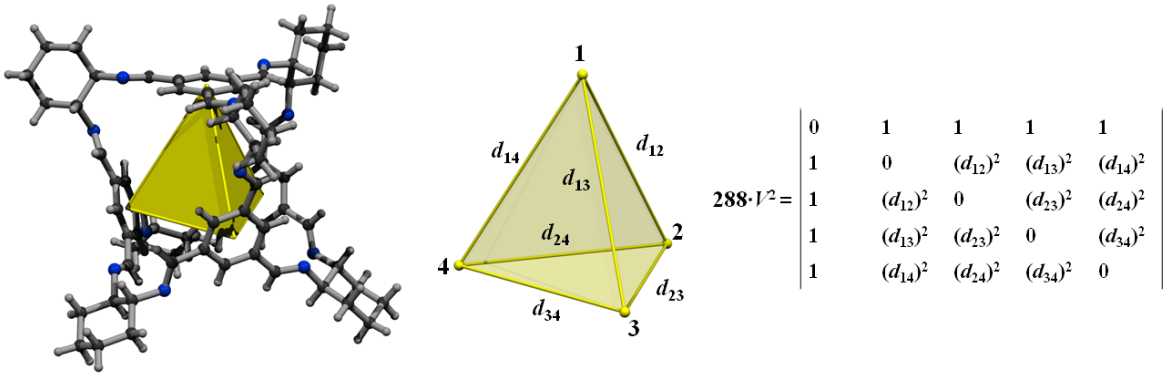

Figure S9. Placement of the tetrahedron inside cage module using the centroids of the four phenyl rings as the vertices (left). Definition of parameters used to calculate tetrahedron volume where spheres 1, 2, 3 and 4 represent the centroids of the four aromatic rings and *d* the distance between (middle). Cayley-Menger determinant used for determining the tetrahedral volume.

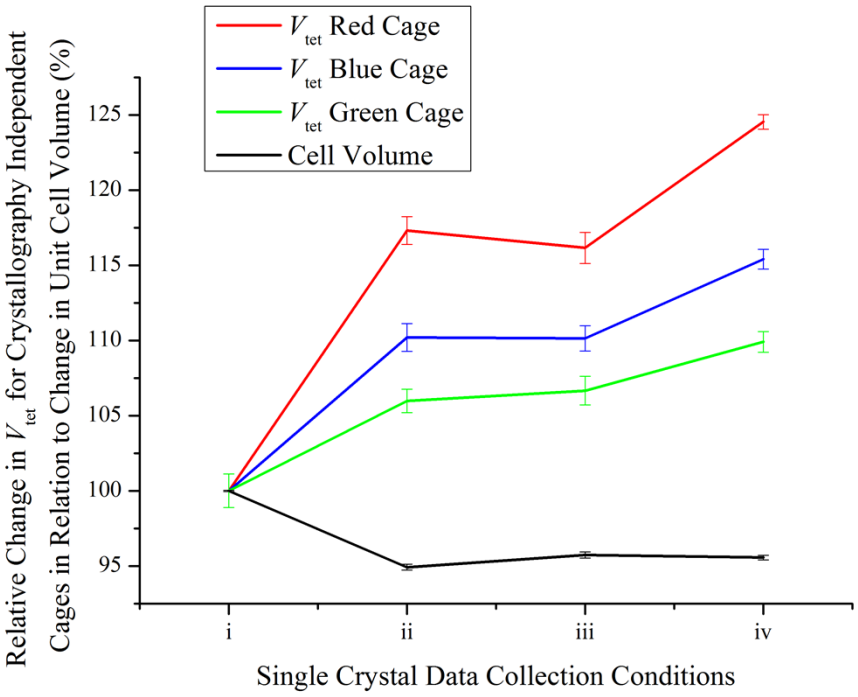

Figure S10. Relative change in V_{tet} for the red, green and blue crystallographically independent cages in relation to the change in the unit cell volume (%) calculated for the single crystal structure **CC3**-*R*·3(Et_2O)·CH_2Cl_2 (i), **CC3**β-300K (ii), **CC3**β-400K (iii) **CC3**β.7.5(N_2) (iv) using the Cayley-Menger determinant.

Table S2. Calculated tetrahedral volumes from the single crystal structures **CC3**-*R*·3(Et_2O)·CH_2Cl_2 (i), **CC3**β-300K (ii), **CC3**β-400K (iii) **CC3**β.7.5(N_2) (iv) using the Cayley-Menger determinant.

	i	ii	iii	iv
Red Cage	31.4 (±0.4) Å^3	36.8 (±0.3) Å^3	36.5 (±0.4) Å^3	39.1 (±0.2) Å^3
Blue Cage	31.4 (±0.4) Å^3	34.6 (±0.3) Å^3	34.6 (±0.3) Å^3	36.2 (±0.2) Å^3
Green Cage	31.4 (±0.4) Å^3	33.3 (±0.3) Å^3	33.5 (±0.3) Å^3	34.5 (±0.2) Å^3

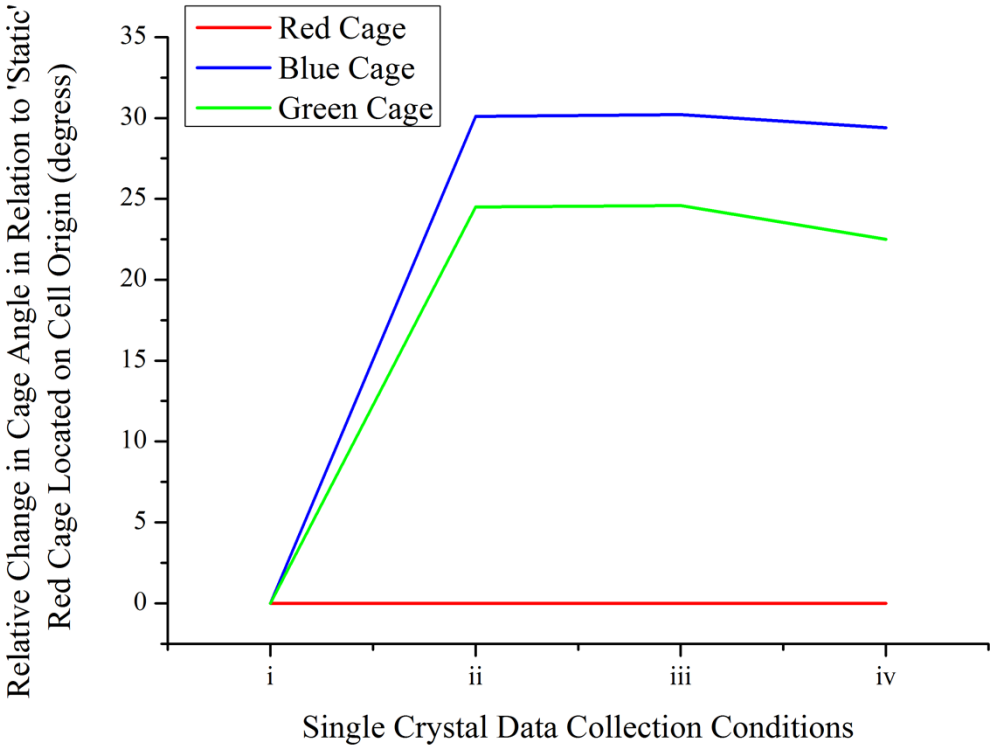

Figure S11. Relative change in z axis rotation for the green and blue crystallography independent cages in relation to the 'static' red cage calculated for the single crystal structure **CC3**-*R*·Et_2O·CH_2Cl_2 (i), **CC3**β-300K (ii), **CC3**β-400K (iii) **CC3**β.7.5(N_2) (iv).

Table S3. Solvent Accessible Surface Area for **CC3**-*R*.3(Et_2O).CH_2Cl_2 and **CC3**β. The solvent surface and accessible solvent surface were calculated in the Materials Studio package[7] using an initial solvent radius of 1.55 Å and ultra-fine, grid spacing of 0.15 Å. Solvent or N_2 were deleted before running the analysis

	CC3-*R*.3(Et_2O).CH_2Cl_2	**CC3**-*R*-β	**CC3**.7.5(N_2)
Solvent Surface			
Occupied Volume (Å^3)	5976.38	6212.81	5999.27
Free Volume (Å^3)	63.07	149.61	80.88
Surface Area (Å^2)	278.49	550.18	339.82
Accessible Solvent Surface			
Occupied Volume (Å^3)	5977.09	6214.86	6019.82
Free Volume (Å^3)	62.36	147.56	60.33
Surface Area (Å^2)	270.27	531.38	252.48

1.4 Gas Sorption Analysis for CC3β

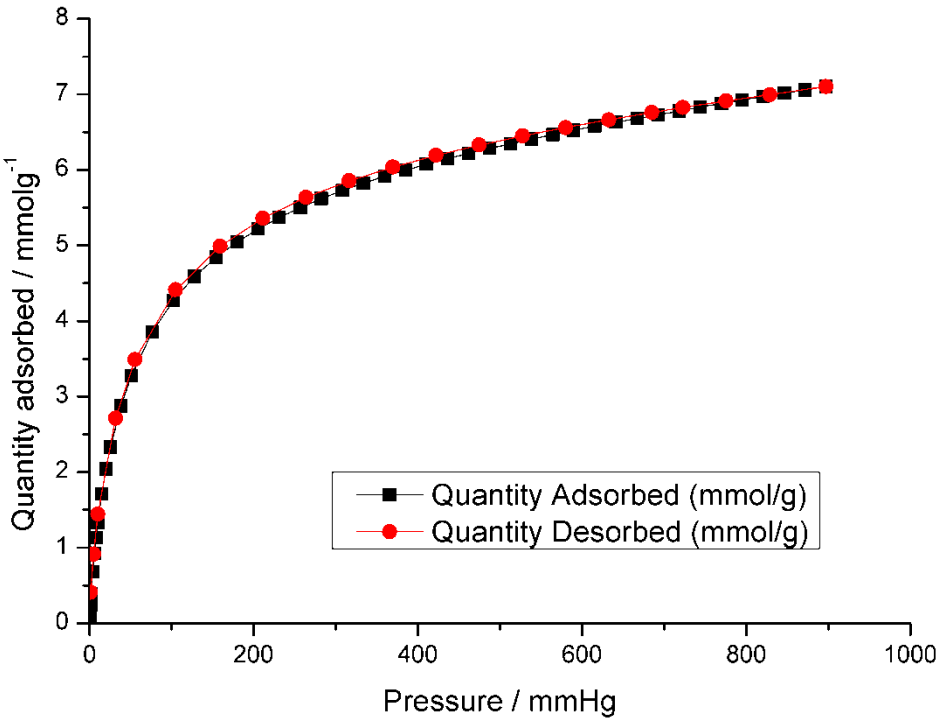

Figure S12. Hydrogen adsorption of **CC3**β at 77 K. Black squares show adsorption, red circles show desorption.

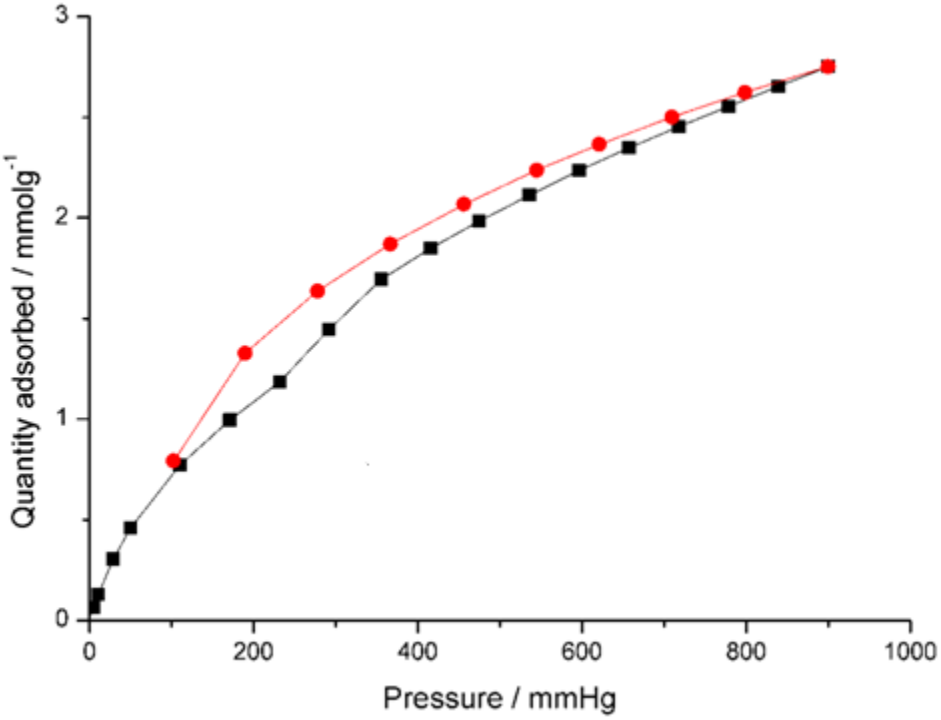

Figure S13. CO_2 adsorption of **CC3**β at 273 K. Black squares show adsorption, red circles show desorption.

1.5 Powder X-ray Diffraction Details

***In situ* nitrogen loading PXRD studies.** The gas adsorption of N_2 in **CC4**α was studied *in situ* using powder diffraction data (PXRD) collected at beamline I11 at Diamond Light Source. Finely ground samples of slowly-crystallised **CC4**α were dried in a vacuum oven at 80 ˚C for 12 hours. These were then packed in 0.7 mm diameter borosilicate capillaries and mounted on the low-pressure capillary gas cell.[8] The sample was exposed to dynamic vacuum (approximately 10^{-5} mbar) and heated to 425 K using an Oxford Cryostream Plus to fully evacuate the sample. Data were collected (λ = 0.826165 Å) using the Mythen-II position sensitive detector (PSD)[9] at 100 K to obtain an initial powder diffraction profile of guest-free **CC4**α. The θ circle was rocked through ±20° to improve powder averaging. Nitrogen gas was dosed into the system in a number of pressure steps, up to a maximum of 10.1 bar (**Figure S14**). The sample was allowed to equilibrate for a minimum of 15 minutes after gas was dosed into the cell. Several datasets were then collected using the PSD to confirm equilibration before increasing the pressure of N_2 in the system. The pressure of nitrogen was reduced in steps before evacuating the gas cell under dynamic vacuum to confirm removal of nitrogen from the pore structure. The cycle of dosing and removing gas at low pressures was repeated to confirm the reproducibility of observed changes (**Figure S15**). Indexing and Le Bail fitting of the PXRD data were carried out using *TOPAS-Academic*.[6] The powder diffraction pattern collected at 100 K under dynamic vacuum was indexed with a body-centred monoclinic cell consistent with three **CC4**-*R* molecules in the asymmetric unit. Le Bail fitting (R_{wp} = 2.22 %, R_p = 1.24 %, χ^2 = 10.4) (**Figure S16**) gave a near orthogonal cell (a = 41.267(1), b = 21.8671(3) c = 23.828(6) Å, β = 89.332(2)°, V = 21500.6(8) Å^3, $I2$) indicating a monoclinic distortion of the single crystal structure reported previously.[6]

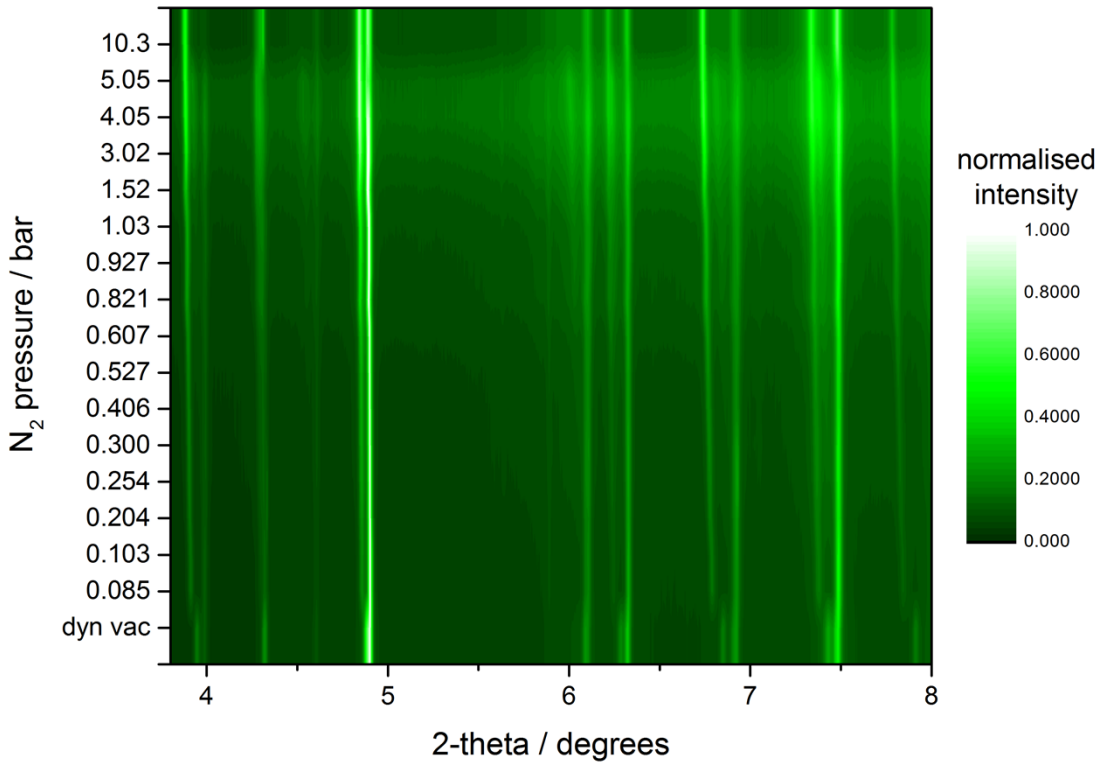

Figure S14. *In-situ* powder X-ray diffraction profile for **CC4**α at varying N_2 loading pressures indicates a possible phase transition between dynamic vacuum and 85 mbar.

Two different plausible cells were proposed for **CC4**α loaded under 85 mbar N_2. The first was a *C*-centred cell (a = 29.9544(5), b = 40.9783(9) c = 22.0910(5) Å, β = 84.925(3)°, V = 27010(1) Å^3, *C*2); an apparent monoclinic supercell of the single crystal unit cell. However, Le Bail refinement (R_{wp} = 2.94 %, R_p = 1.49 %, χ^2 = 13.5) showed the fit of low angle diffraction peaks was not ideal (**Figure S17**(**a**)) and the combination of volume and symmetry elements was unlikely to be compatible with the molecular structure of **CC4**-*R*. The second possible cell (a = 10.9627(2), b = 23.7547(4) c = 23.8977(7) Å, α = 118.896(2)° β = 89.332(2)°, γ = 90.3959(2)°, V = 5447.7(2) Å^3, *P*1) was a direct triclinic distortion of the reported structure, consistent with three full **CC4**-*R* molecules in the asymmetric unit. The Le Bail fit using this cell remains less than satisfactory (R_{wp} = 2.41 %, R_p = 1.40 %, χ^2 = 11.1) (**Figure S17**(**b**)), particularly in the range 7.7° ≤ 2θ ≤ 11.6°. While improved fits of the data can be obtained with significantly larger cells, they also require a far larger number of parameters. Therefore, this triclinic cell is proposed as the best representation of periodicity and symmetry currently obtainable from this dataset. However, the actual structure is likely to be more complex than can be characterised at present.

Analogous *in situ* N_2 loading experiments were performed for **CC3**β up to a maximum nitrogen pressure of 1.04 bar (**Figure S18**). A concerted shift of peaks at low pressure (65 mbar) was observed,

commensurate with an expansion of lattice parameters on the initial adsorption of nitrogen into the structure. There is no evidence of the structural transition observed for **CC4**α upon loading under low pressures of nitrogen.

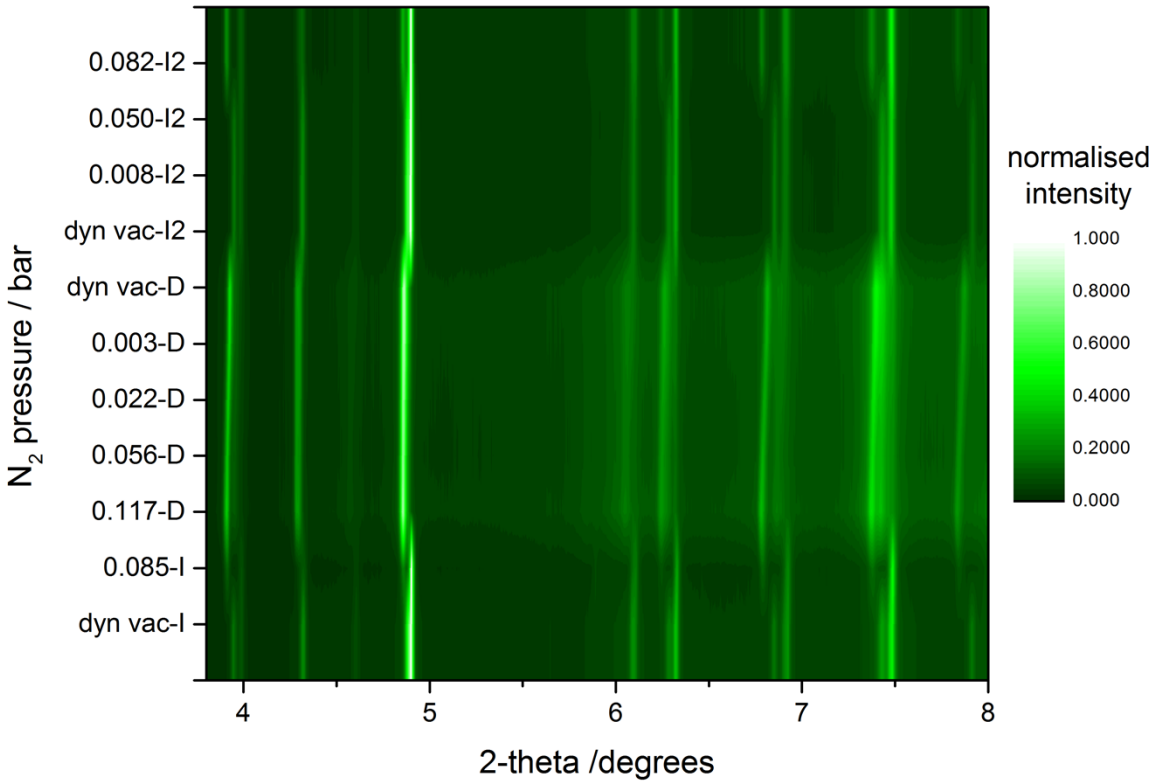

Figure S15. Powder X-ray diffraction data for **CC4**α during *in situ* nitrogen gas loading and evacuation. A transition is observed after exposing fully evacuated **CC4**α to 85 mbar N_2. The initial powder diffraction pattern for the empty host is subsequently only regained after dynamic vacuum was applied and the temperature was raised to 293 K. The first transition was then reproduced at a pressure between 0.050 and 0.082 mbar.

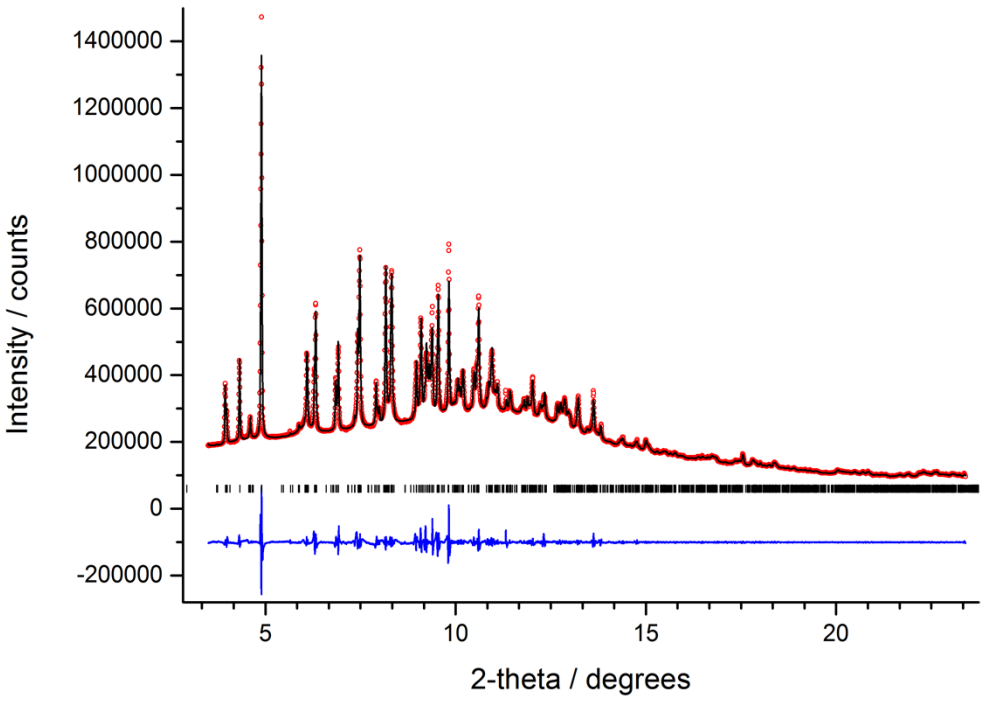

Figure S16. Final observed (red circles), calculated (black line) and difference PXRD profiles for Le Bail refinement (R_{wp} = 2.22 %, R_p = 1.24 %, χ^2 = 10.4) of **CC4**α under dynamic vacuum at 100 K (*a* = 41.267(1), *b* = 21.8671(3), *c* = 23.828(6) Å, *β* = 89.332(2)°, *V* = 21500.6(8) Å^3, *I*2). Reflection positions are also marked.

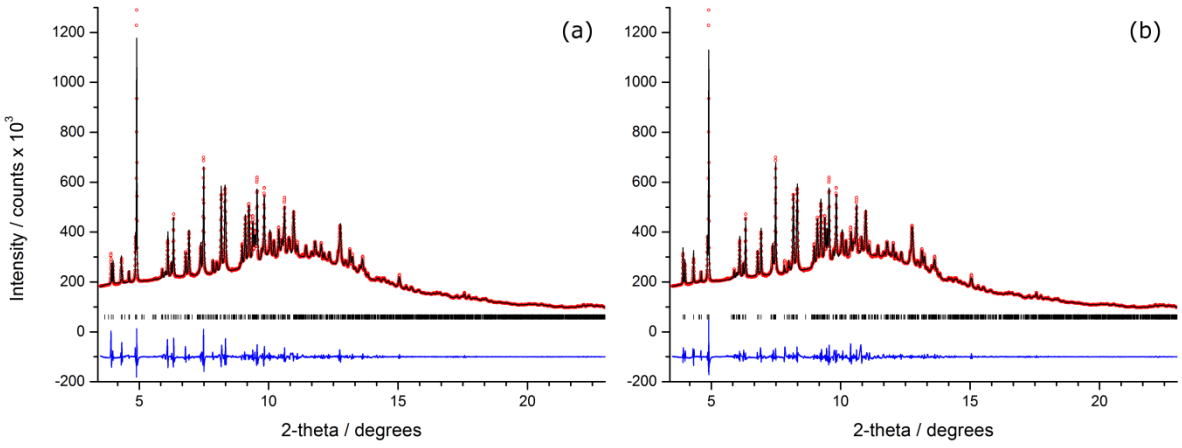

Figure S17. Final observed (red circles), calculated (black line) and difference PXRD profiles for (a) Le Bail refinement (R_{wp} = 2.94 %, R_p = 1.49 %, χ^2 = 13.5) of **CC4**α under 85 mbar N2 at 100 K based on a monoclinic cell (*a* = 29.9544(5), *b* = 40.9783(9), *c* = 22.0910(5) Å, *β* = 84.925(3)°, *V* = 27010(1) Å^3, *C*2); (b) Le Bail refinement (R_{wp} = 2.41 %, R_p = 1.40 %, χ^2 = 13.5) of **CC4**α under 85 mbar N_2 at 100 K based on a triclinic cell (*a* = 10.9627(2), *b* = 23.7547(4), *c* = 23.8977(7) Å, *α* = 118.896(2)° *β* = 89.332(2)°, *γ* = 90.3959(2)°, *V* = 5447.7(2) Å^3, *P*1). Reflection positions are also marked.

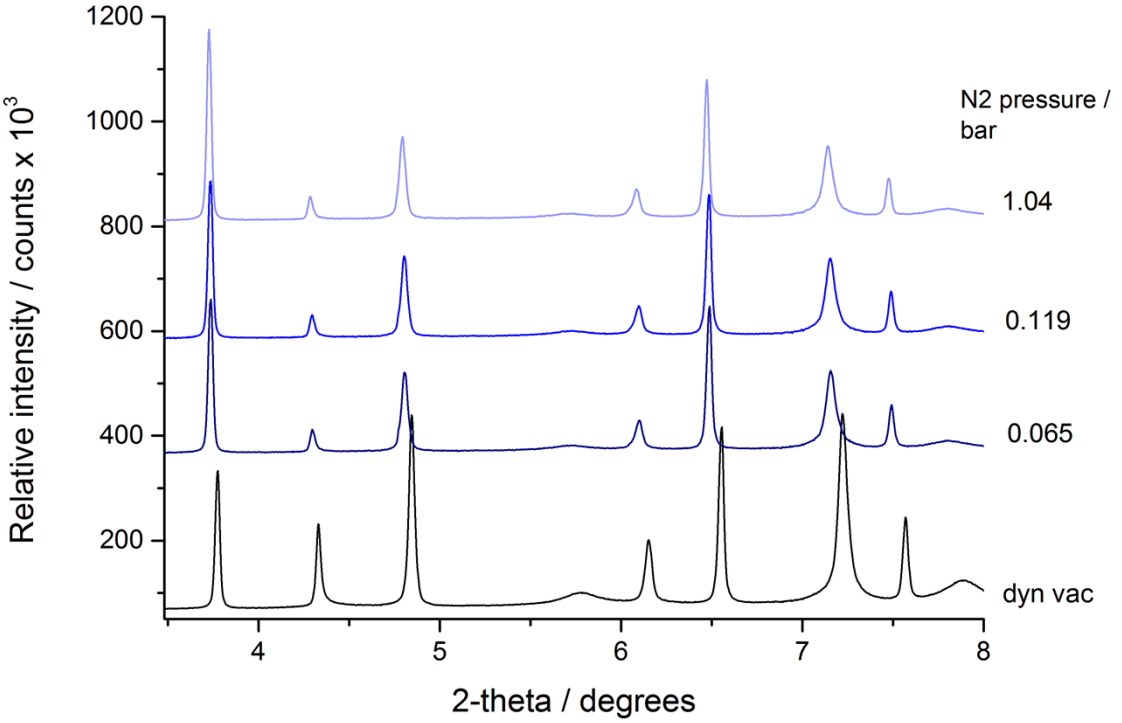

Figure S18. *In-situ* powder X-ray diffraction profile for **CC3**β loaded under variable pressures of nitrogen. A uniform peak shift is observed upon dosing with 65 mbar of N_2. However, there is no evidence of a low-pressure structural transition.

1.6 CC4 solvent screen

A total of 30 organic solvents (Table S4) were trialled as possible directing solvents to search for novel crystalline forms of **CC4**. For each co-solvent, 2 cm^3 was layered onto 3 cm^3 of a solution of **CC4**-*R* in dichloromethane (3.871 mmol, 4.0 mg cm^{-3}) using an automated ChemSpeed Technologies Swing platform. The solvents were allowed to fully evaporate and the resultant solid materials were analysed by PXRD.

Table S4. Co-solvents used in screen for new polymorphs of **CC4**-*R*. Only *p*-xylene yields **CC4**β.

Dichloromethane	Diethyl ether	Acetonitrile
Chloroform	Acetone	Ethanediol
1,2-Dichloroethane	*ortho*-Xylene	Cyclohexane
Toluene	*para*-Xylene	Dimethylacetamide
Ethanol	*meta*-Xylene	Propanol
Isopropanol	*n*-Hexane	Methanol
Dimethylsulfoxide	Heptane	Di-isopropyl ether
Tetrahydrofuran	Butanol	Methyl acetate
1,4-Dioxane	Octanol	Ethyl acetate
Dimethylformamide	Mesitylene	Pentane

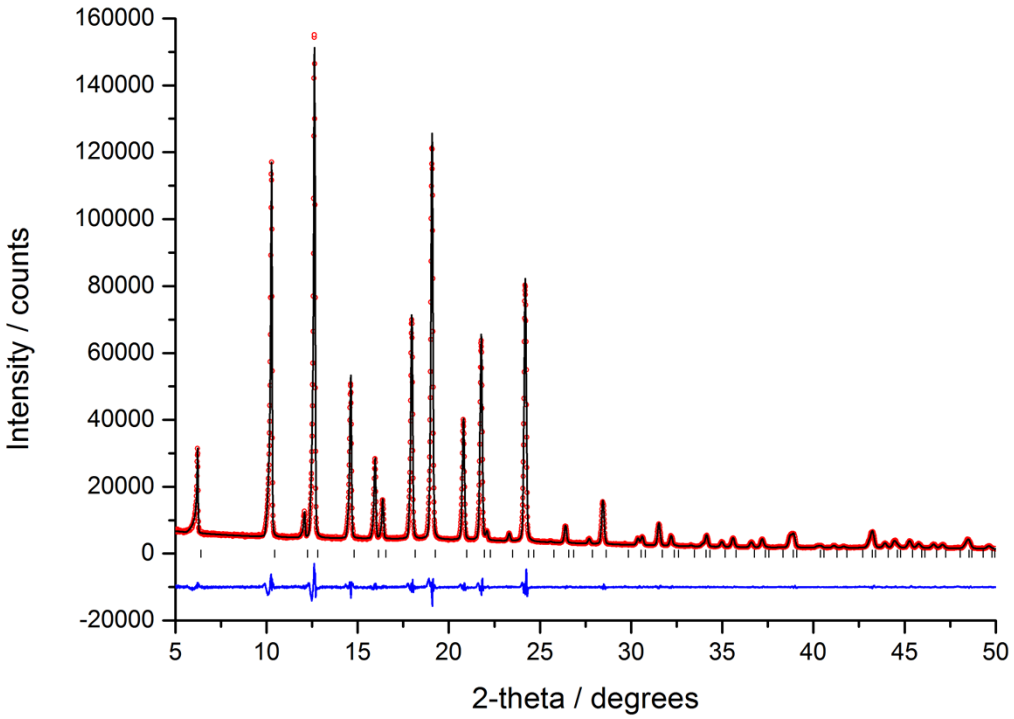

Figure S19. Final observed (red circles), calculated (black line) and difference PXRD profiles for Le Bail refinement (R_{wp} = 4.30 %, R_p = 3.10 %, χ^2 = 3.34) of **CC4**β (*a* = 23.9320(3) Å, *V* = 13706.9(5) Å^3, *F*4$_1$32). Reflection positions are also marked.

1.7 Crystallography for CC4β

CC4-*R* (357 mg, 0.35 mmol) was dissolved in CH_2Cl_2 (20 mL), to this solution *para*-xylene (30 mL) was layered on top. The solvent mixture was allowed to slowly evaporate, after ~ 10 days plate shaped crystals of **CC4**-*R*·3(C_8H_{10})·2(H_2O) were found to have crystallised from solution. The solvent mixture was allowed to slowly evaporate until only the last 5 mL remained, this was decanted and isolated crystalline material was dried in a vacuum oven at 90 °C for 18 hours. Isolated yield after evacuation 276 mg: 77 %.

Supplementary single crystal structure data for **CC4**β was included in a previous publication.[10] In the previous publication the crystal structure of **CC4**β was compared to predicted polymorphs for homochiral **CC4**-*R*.

Refinement Notes for CC4-*R*·3(C_8H_{10})·2(H_2O). The structure was solved and refined in the chiral orthorhombic space group $P2_12_12_1$. The crystals were weakly diffracting and a 0.85 Å resolution limit was applied during refinement. The asymmetric unit for **CC4**-*R*·3(C_8H_{10})·2(H_2O) is composed of one

complete **CC4**-*R* molecules, three *para*-xylene molecules; and two water molecules. The water molecules were refined isotropically without protons, however these were included in the refined formula unit. One of the *para*-xylene molecules was disordered over two positions. For this molecule the atoms were refined isotropically and atoms which shared equivalent coordinates were refined with the constraint EADP. In addition, for this molecule, DFIX and SADI restraints were used during final stages of refinement in addition to a group FLAT restraint. The other two *para*-xylene molecules were refined anisotropically; one of these was refined with a rigid bond restraint (DELU). For a displacement ellipsoid plot of the asymmetric unit see **Figure S20**.

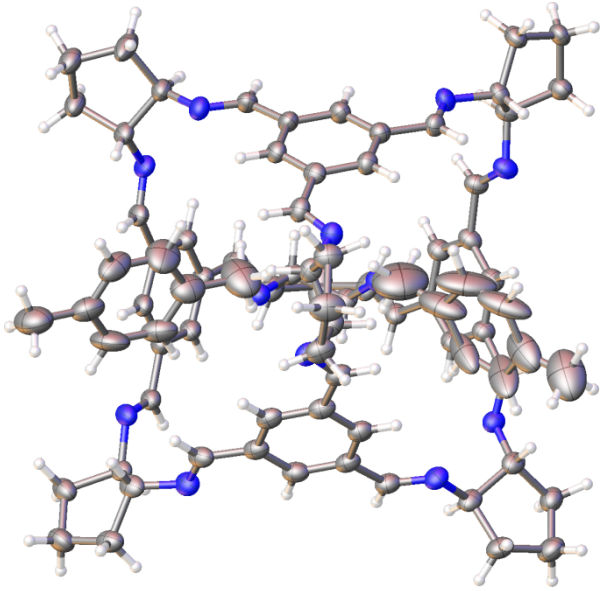

Figure S20. Asymmetric unit from the single crystal structure **CC4**-*R*·3(C_8H_{10})·2(H_2O). Isotropically refined *para*-xylene and H_2O omitted for clarity.

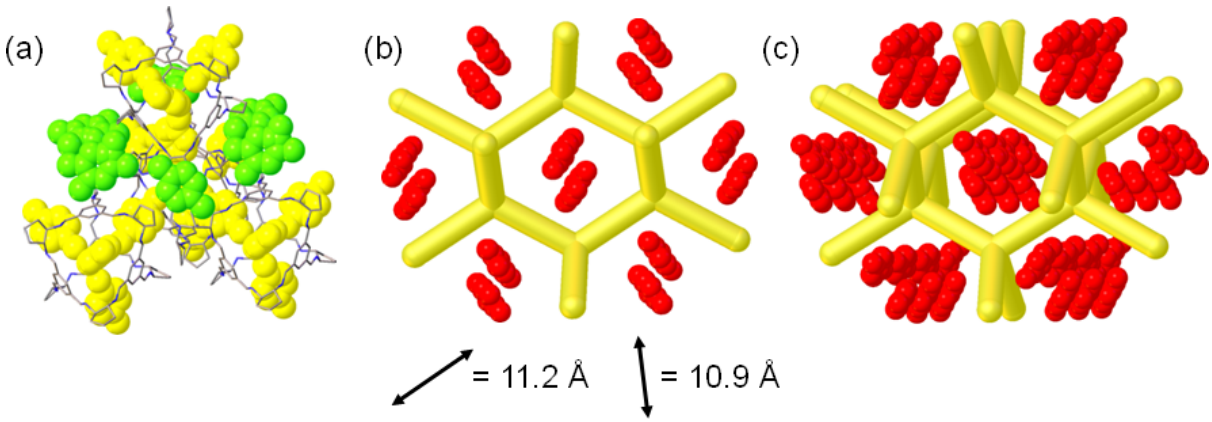

Figure S21. Graphical representation of the crystal packing for **CC4**-*R*·3(C_8H_{10})·2(H_2O), *para*-xylene solvate shown in space filling format. Diamondoid arrangement of window positioned *para*-xylene solvate shown in yellow, extrinsically positioned *para*-xylene solvate shown in green (a). Connectivity between **CC4**-*R* cavities shown as yellow line, with approximate cage centre to cage centre distances below, extrinsically positioned *para*-xylene solvate shown in red (b + c).

Single Crystal Experimental Procedure. A single crystal was selected from a sealed sample vial containing residual *para*-xylene and CH_2Cl_2 and immediately flash frozen under a dry nitrogen gas

steam at 100 K. A full data set was recorded, this was refined as **CC4**-*R*·3(C_8H_{10})·2(H_2O). The same single crystal was very gradually heated under a dry nitrogen gas flow eventually to 350 K; see **Figure S22** for variable temperature plot. Analysis of the data set recorded at 350 K revealed a single-crystal to single-crystal transformation had occurred transforming the crystal symmetry to the chiral cubic space group $F4_132$, with no notable solvent positions in the crystal lattice. This data set is referred to hereafter as **CC4**β.

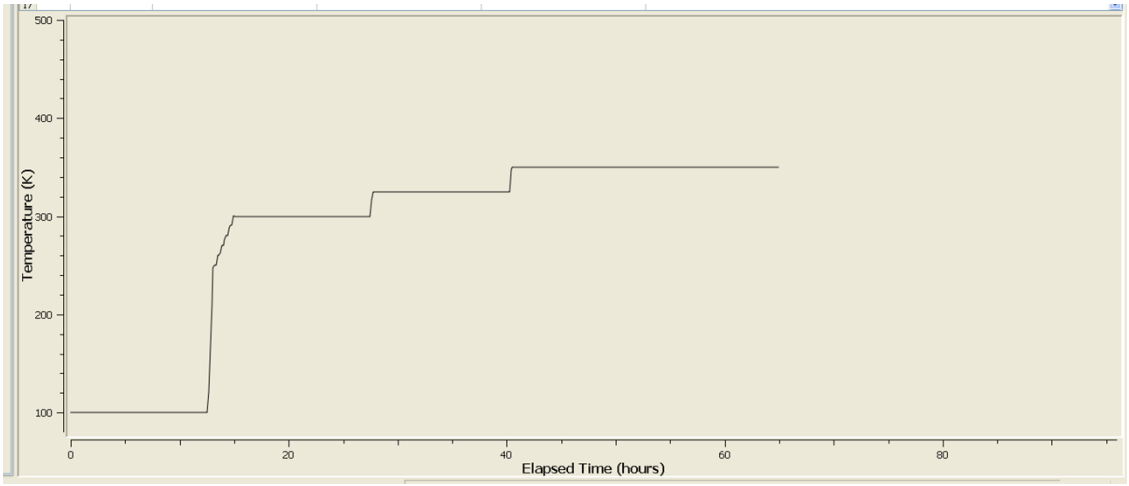

Figure S22. Variable temperature plot from a single crystal study carried out with **CC4**-*R*·3(C_8H_{10})·2(H_2O).

Refinement Notes for CC4β. Desolvation of **CC4**-*R*·3(C_8H_{10})·2(H_2O) to afford **CC4**β is accompanied by a significant structural change as discussed in the main text. The structure of **CC4**β was solved and refined in the chiral cubic space group $F4_132$. A 1.1 Å resolution limit was applied during integration. The asymmetric unit for **CC4**β is composed of one twelfth of a **CC4**-*R* molecule. No restraints were used during refinement. For a displacement ellipsoid plot of the asymmetric unit see **Figure S23**.

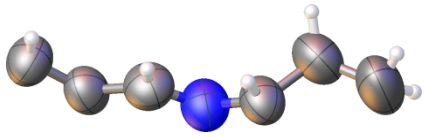

Figure S23. Displacement ellipsoid plot of the asymmetric unit from the single crystal structure **CC4**β.

Table S5. Single crystal X-ray crystallography refinement details for **CC4**-*R*·3(C_8H_{10})·2(H_2O) and **CC4**β

Sample Reference	**CC4**-*R*·3(C_8H_{10})·2(H_2O)	**CC4**β
Collection *T*	100 K	350 K
Formula	$C_{90}H_{106}N_{12}O_2$	$C_{66}H_{72}N_{12}$
Mr	1387.87	1033.36
Crystal Size (mm)	0.41 x 0.17 x 0.04	0.41 x 0.17 x 0.04
Crystal Colour	Colourless	Colourless
Crystal System	Orthorhombic	Cubic
Space Group	$P2_12_12_1$	$F4_132$
a [Å]	16.749(2)	24.242(9)
b [Å]	19.254(2)	-
c [Å]	25.342(3)	-
V [Å^3]	8172(1)	14246(9)
Z	4	8
D_{calcd} [g cm^{-3}]	1.128	0.964
μ[mm^{-1}]	0.069	0.058
F(000)	2984	4416
2θ range [°]	3.42 – 49.42	2.90 – 37.62
Reflections collected	134283	26833
Independent reflections, R_{int}	13923, 0.0690	480, 0.1241
Obs. Data [I > 2σ]	12428	408
Data / restraints / parameters	13923 / 58 / 887	480 / 0 / 60
Final R1 values (I > 2σ(I))	0.0698	0.1146
Final *wR*(F^2) values ($I > 2\sigma(I)$)	0.1982	0.2692
Final R1 values (all data)	0.0778	0.1270
Final wR(F2) values (all data)	0.2088	0.2904
Goodness-of-fit on F^2	1.060	1.338
Largest diff. peak and hole [e.A^{-3}]	0.682 / -0.541	0.956 / -0.191
CCDC	991219	991218

1.8 Gas Sorption Analysis for CC4β

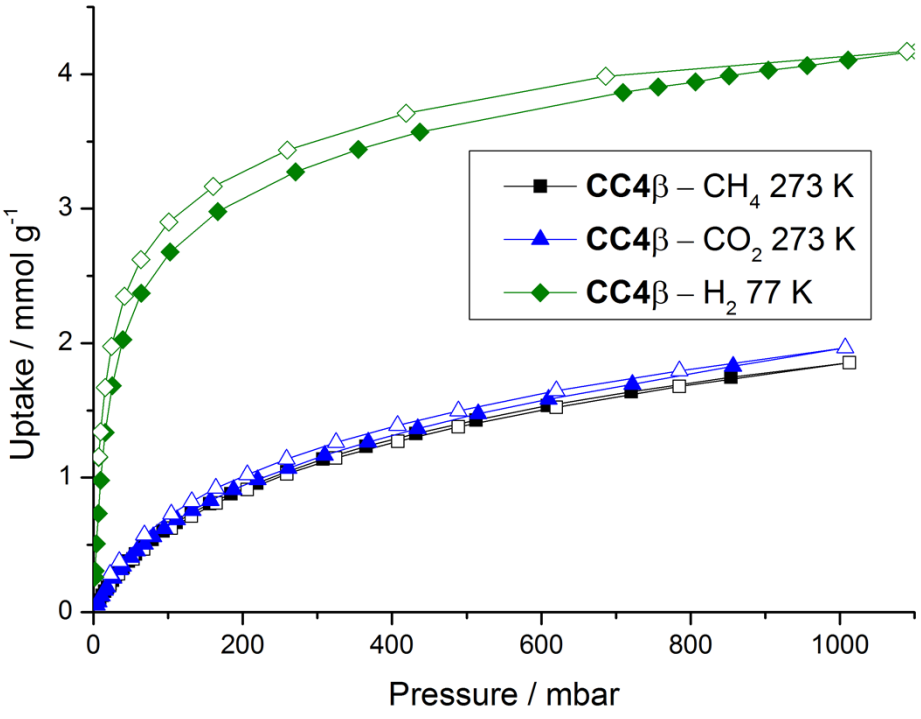

Figure S24. Sorption isotherms, recorded for **CC4**β. Closed symbols show the adsorption isotherm, and open symbols show the desorption isotherm.

1.9 References

1. T. Tozawa, J. T. A. Jones, S. I. Swamy, S. Jiang, D. J. Adams, S. Shakespeare, R. Clowes, D. Bradshaw, T. Hasell, S. Y. Chong, C. Tang, S. Thompson, J. Parker, A. Trewin, J. Bacsa, A. M. Z. Slawin, A. Steiner and A. I. Cooper, *Nat Mater.*, 2009, **8**, 973-978.
2. T. Mitra, X. Wu, R. Clowes, J. T. A. Jones, K. E. Jelfs, D. J. Adams, A. Trewin, J. Bacsa, A. Steiner and A. I. Cooper, *Chem. –Eur. J.*, 2011, **17**, 10235-10240.
3. G. M. Sheldrick, *(University of Göttingen, Germany)*, 2008.
4. G. M. Sheldrick, *Acta Cryst. Sect. A*, 2008, **64**, 112-122.
5. O. V. Dolomanov, L. J. Bourhis, R. J. Gildea, J. A. K. Howard and H. Puschmann, *J. Appl. Cryst.*, 2009, **42**, 339-341.
6. A. A. Coelho, TOPAS Academic, Version 4.1, Coelho Software, 2007.
7. Accelrys; Accelrys Software Inc.:San Diego, 2011.
8. J. E. Parker, J. Potter, S. P. Thompson, A. R. Lennie and C. C. Tang, *Materials Science Forum*, 2012, **706 - 709**, 1707-1712.
9. S. P. Thompson, J. E. Parker, J. Marchal, J. Potter, A. Birt, F. Yuan, R. D. Fearn, A. R. Lennie, S. R. Street and C. C. Tang, *J. Sync. Rad.*, 2011, **18**, 637-648.
10. E. O. Pyzer-Knapp, H. P. G. Thompson, F. Schiffmann, K. E. Jelfs, S. Y. Chong, M. A. Little, A. I. Cooper and G. M. Day, *Chem. Sci.*, 2014, **5**, 2235-2245.